An Analysis of Isostasy in the World's Oceans 1. Hawaiian-Emperor Seamount Chain

A. B. WATTS

Lamont-Doherty Geological Observatory and Department of Geological Sciences Columbia University, Palisades, New York 10964

Cross-spectral techniques have been used to analyze the relationship between gravity and bathymetry on 14 profiles of the Hawaiian-Emperor seamount chain. The resulting filter or transfer function has been used to evaluate the state of isostasy along the chain. The transfer function can be best explained by a simple model in which the oceanic lithosphere is treated as a thin elastic plate overlying a weak fluid. The best-fitting estimate of the elastic thickness of the plate is in the range 20–30 km. Analysis of individual profiles shows significant differences in the elastic thickness along the seamount chain. Relatively low estimates of the elastic thickness were obtained for the Emperor Seamounts north of 40°N, and relatively high estimates for the Emperor Seamounts south of 40°N and the Hawaiian Ridge. These differences cannot be explained by a simple model in which there is a viscous reaction to the seamount loads through time. The best explanation is a simple model in which the elastic thickness depends on age and hence temperature gradient of the lithosphere. The low values can be explained if the Emperor Seamounts north of 40°N loaded a relatively young hot plate, and the high values can be explained if the Emperor Seamounts south of 40°N and the Hawaiian Ridge loaded a relatively old cold plate. These estimates of the elastic thickness along with determinations from other loads on the Pacific lithosphere suggest that the elastic thickness corresponds closely to the 450 ± 150°C isotherm, based on simple cooling models. Thus the large deformations and associated flexural stresses (>1 kbar) at seamount loads do not appear to change appreciably through time. This conclusion is in agreement with subsidence data along the seamount chain and with some gravity observations in the continents.

INTRODUCTION

The theory of plate tectonics is based on the concept of a strong rigid lithosphere which overlies a weak asthenosphere. This simple model for the mechanical properties of the outer layers of the earth has been known since the pioneering studies of *Barrell* [1914] and *Gunn* [1943]. The main argument (for example, *Jeffreys* [1962]) for the existence of a strong lithosphere has come from observations that features on the earth's surface such as mountain ranges have been supported for many millions of years. The existence of a weak asthenosphere is implied from observations that large loads on the earth's surface such as deltas are gravitationally compensated. The compensation for these loads is assumed to be accomplished by flow in the underlying weak layer.

The main evidence for the long-term ($>10^6$ years) mechanical properties of the lithosphere, however, has come from studies of the way it responds to surface loads. Studies have now been made of the deformation of the oceanic lithosphere caused by the weight of linear seamount chains [*Walcott, 1970a*; *Watts and Cochran, 1974*] and individual isolated seamounts [*Watts et al., 1975*]. In addition, a number of studies have been made of the deformation of the oceanic lithosphere approaching a deep-sea trench [*Hanks, 1971*; *Watts and Talwani, 1974*; *Dubois et al., 1975*; *Caldwell et al., 1976*; *Parsons and Molnar, 1976*]. It now appears that in a number of cases the oceanic lithosphere responds to long-term surface loads in a manner similar to an elastic plate overlying a weak fluid.

An important parameter in loading studies is the flexural rigidity, which is a measure of the stiffness of the lithosphere. The flexural rigidity determines both the amplitude and the wavelength of flexure due to a surface load. By comparing topography and gravity anomaly evidence of flexure to the plate models, a number of estimates of the flexural rigidity of the lithosphere have been made. In the oceans the rigidity is in the range 10^{28}–10^{31} dyn cm and in the continents in the range 10^{29}–10^{31} dyn cm [*Walcott, 1970a, b*; *Watts and Cochran, 1974*; *Watts et al., 1975*; *Haxby et al., 1976*]. Since the flexural rigidity is determined mainly by the elastic thickness, these ranges imply a thickness of 5–40 km for the oceanic lithosphere and 15–45 km for the continental lithosphere. The elastic thickness of the lithosphere is therefore much less than the thermal or seismic thickness and corresponds to the depth to which materials behave elastically on long time scales.

One of the most studied surface loads on the oceanic lithosphere is the Hawaiian-Emperor seamount chain in the Pacific Ocean. The earliest gravity measurements [*Vening Meinesz, 1941*] suggested that the load of the seamount chain was not supported according to the Airy model of isostasy but was regionally supported. *Gunn* [1943], *Walcott* [1970*a*], and *Watts and Cochran* [1974] have shown that gravity data are generally consistent with a simple model in which the lithosphere supports the load in a manner similar to a thin elastic plate overlying a weak fluid layer. The seamount chain is a particularly satisfactory load for flexure studies. First, the ages of individual seamounts increase along the chain [*Clague and Jarrard, 1973*; *Dalrymple et al., 1974*], allowing any effects of a viscous reaction of the lithosphere to the load to be examined. Second, the chain is located in the center of the Pacific plate away from the complexities of plate boundaries.

Previous studies of the Hawaiian-Emperor seamount chain by *Walcott* [1970*a*] and *Watts and Cochran* [1974] utilized mainly gravity and bathymetry data. The general procedure was to determine the load from the visible topography and then compute the deformation of the lithosphere by using simple elastic or viscoelastic models. The gravity effect of the load and its compensation were then computed for different values of the flexural rigidity and compared with observed free air gravity anomaly profiles. The value of the flexural rigidity which best minimized the sums of the squares of the residuals between observed and computed gravity anomalies was determined. However, one problem with this approach was that

Paper number 8B0752.
0148-0227/78/128B-0752$01.00

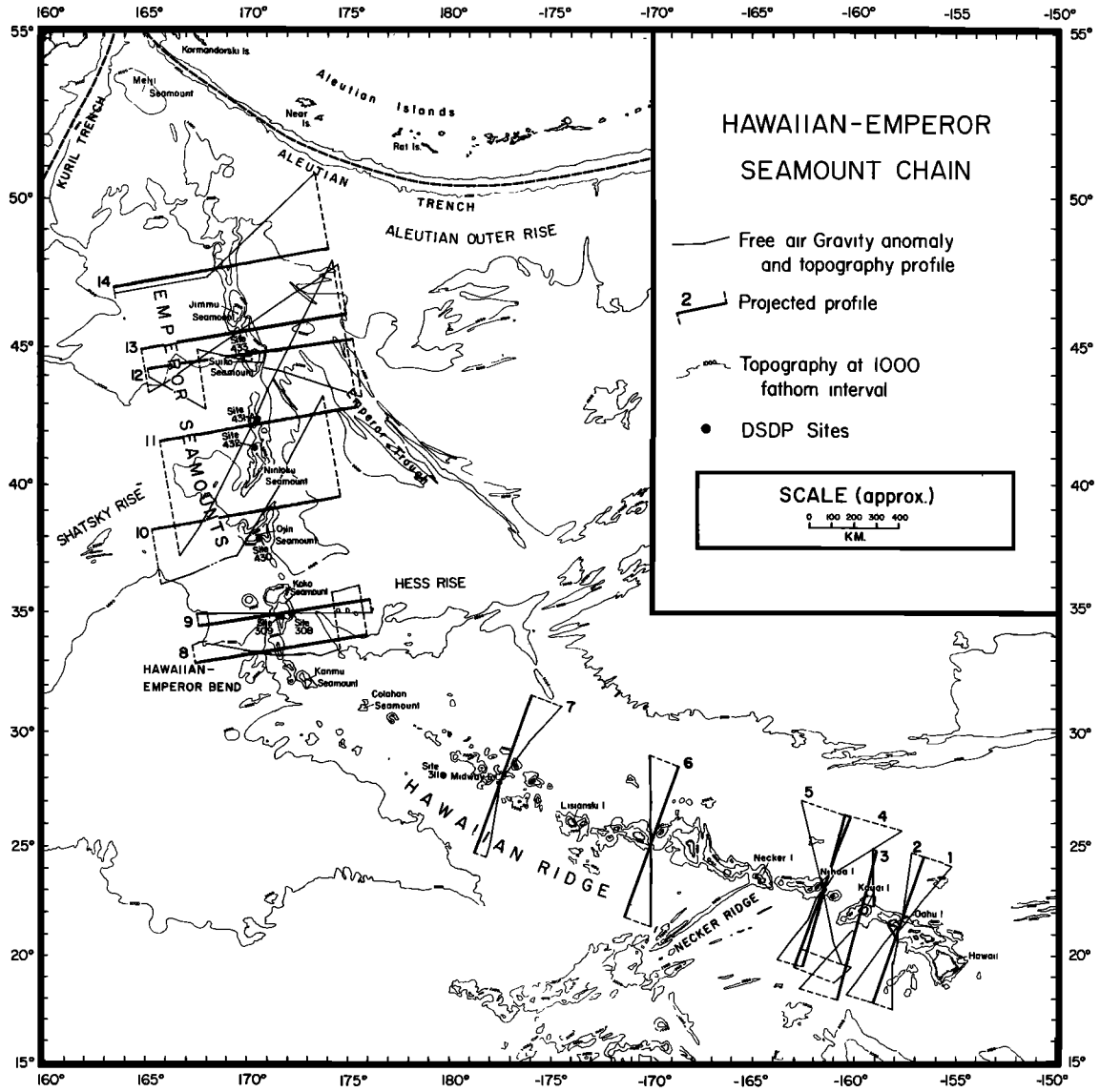

Fig. 1. Location of free air gravity anomaly and bathymetry profiles used in this study. The thin lines indicate the actual ship track, and the heavy lines indicate the profile the data along each track were projected onto. The bathymetry is based on *Chase et al.* [1970]. DSDP sites located on or near the seamount chain are shown as solid circles.

amplitude rather than wavelength was emphasized in the sums of the squares computation.

A more quantitative approach to understanding isostasy is to use linear transfer function techniques which examine the relationship of gravity and elevation as a function of wavelength [*Neidell*, 1963; *Dorman and Lewis*, 1970; *Lewis and Dorman*, 1970; *McKenzie and Bowin*, 1976]. The transfer function for a region contains information on the mechanism of isostasy. The advantage of these techniques is that they use observational data and are not based on a particular model of isostasy. The transfer function can, however, be interpreted in terms of different models of isostasy and in some cases may be used to distinguish among them.

The main limitation with the previous studies by *Dorman and Lewis* [1970], *Lewis and Dorman* [1970], and *McKenzie and Bowin* [1976] is that they have been applied over rather broad regions comprising different tectonic provinces. *Lewis and Dorman* [1970] and *Dorman and Lewis* [1970] determined a transfer function for the entire continental United States. The resulting function included the lithospheric response to surface loads for a number of different geological provinces. Although *Lewis and Dorman* [1970] interpreted the function in terms of the Airy model, *Walcott* [1976] and *Banks et al.* [1977] interpreted it in terms of a plate model. *Walcott* [1976] pointed out that competing effects from the Basin and Range and Precambrian (Grenville) shield provinces could be distinguished. *McKenzie and Bowin* [1976] determined a transfer function for the Atlantic Ocean by using two long surface ship gravity and bathymetry profiles. The resulting function included the lithospheric response to a number of different geological features on the sea floor. Most of these features, however, were formed at or near a mid-ocean ridge crest, and *McKenzie and Bowin* [1976] were able to interpret the transfer function in terms of a single geological process occurring in the axial region of mid-ocean ridge crests.

The purpose of this paper is to present a method of quantitatively analyzing the state of isostasy at a single geological feature and to apply it to a study of the Hawaiian-Emperor seamount chain. The method is based on linear transfer techniques described previously by *Dorman and Lewis* [1970],

Lewis and Dorman [1970], and *McKenzie and Bowin* [1976]. The main differences are that cross-spectral techniques are used to compute the transfer function and that many profiles of gravity and bathymetry over the same geological feature are used to obtain smooth spectral estimates. There are three main objectives of the study: (1) to determine the transfer function which best describes the relationship between gravity and bathymetry along the chain, (2) to interpret the resulting transfer function in terms of simple models of isostasy, and (3) to use the preferred model of isostasy to provide constraints on the long-term ($>10^6$ years) mechanical properties of the oceanic lithosphere.

DATA REDUCTION

This study utilizes 14 surface ship free air gravity anomaly and bathymetry profiles (Figure 1) of the Hawaiian-Emperor seamount chain. A summary of the instruments and navigation used during each profile is presented in Table 1.

The overall accuracy of the gravity data depends on the type of instruments and navigation used. Studies of discrepancies of intersecting ship's tracks show small values (0–5 mgal) except for profile 5 which was systematically in error by +10 mgal. This error was attributed to an incorrect base station value, and the profile was corrected by +10 mgal. Although systematic errors are important, errors also arise in gravity measurements owing to poor navigation and horizontal accelerations acting on the ship. In general, those cruises which used the improved version of the Gss 2 sea gravimeter or the MIT instrument with satellite navigation should be accurate to about 2–5 mgal. However, somewhat larger errors would be expected for cruises which used the gimbal-mounted LaCoste-Romberg gravimeter or celestial navigation.

The gravity anomalies were reduced to the International Reference Ellipsoid (flattening of 1/297.0). However, the choice of a reference ellipsoid is not important, since the mean and trend were removed before the data were Fourier transformed.

The ships tracks along which the profiles were obtained are shown in Figure 1. Gravity and bathymetry profiles projected normal to the local trend of the seamount chain are shown in Figure 2.

THEORY OF THE METHOD

This study utilizes time series techniques of analyzing gravity and bathymetry similar to those previously used by *Lewis and Dorman* [1970], *Dorman and Lewis* [1970], and *McKenzie and Bowin* [1976].

We require a filter which when applied to an observed bathymetry profile converts it to a series which resembles observed gravity. In the space domain this process consists of convolving an impulse response (or Green's function) $f(x)$ with the bathymetric profile $b(x)$:

$$g(x) = f(x) * b(x) \tag{1}$$

In the wave number domain this is equivalent to a simple multiplication:

$$G(k_n) = Z(k_n) \cdot B(k_n) \tag{2}$$

where $G(k_n)$, $Z(k_n)$, and $B(k_n)$ are the discrete Fourier transforms of $g(x)$, $f(x)$, and $b(x)$ and k_n is the wave number $(k_n) = 2\pi/\lambda$. Thus

$$Z(k_n) = [G(k_n)]/[B(k_n)] \tag{3}$$

This is similar to the form of the transfer function or admittance used by *Dorman and Lewis* [1970] and *Lewis and Dorman* [1970]. In the presence of noise a better estimate is given by *McKenzie and Bowin* [1976]:

$$Z(k_n) = [G(k_n) \cdot B(k_n)^*]/[B(k_n) \cdot B(k_n)^*] \tag{4}$$

where * indicates the complex conjugate. In this case the admittance is given by the cross spectrum of gravity and bathymetry divided by the power spectrum of the bathymetry.

TABLE 1. Summary of Navigation and Instrumentation

Profile	Ship	Cruise and Leg*	Instruments	Navigation	Cross-coupling	Comments
1	*Robert D. Conrad*	1204	Gss 2†	satellite	no	
	Vema	2004	Gss 2	celestial	no	
2	*Vema*	2105	Gss 2	celestial	no	
	Robert D. Conrad	1220	Gss 2	satellite	yes	
3	*Vema*	2811	Gss 2	satellite	yes	
	Vema	3211	Gss 2	satellite	yes	
4	*Robert D. Conrad*	1211	Gss 2	satellite	no	
	Robert D. Conrad	1301	Gss 2	satellite	yes	
5	*Eltanin*	EL30	Gss 2	satellite	yes	
6	*Hakuhō Maru*	HM68	TSSG‡	celestial	···	Leg filtered to remove short wavelength 'noise'
7	*Vema*	2405	Gss 2	satellite	yes	
	Vema	2005	Gss 2	celestial	no	
	Oceanographer	P004	LaCoste-Romberg		···	
8	*Vema*	3212	Gss 2	satellite	yes	
9	*Argo*	LU01	LaCoste-Romberg	celestial	···	
10	*Robert D. Conrad*	1219	Gss 2	satellite	yes	
11	*Robert D. Conrad*	1108	Gss 2	satellite	no	
12	*Hakuhō Maru*	KH68	TSSG	celestial	···	
	Robert D. Conrad	1219	Gss 2	satellite	yes	
13	*Robert D. Conrad*	1207	Gss 2	satellite	no	
14	*Vema*	2006	Gss ?	celestial	no	

*Cruise and leg (for example, for profile 1, 1204 is Conrad cruise 12, leg 4).
†Graf-Askania Gss 2 (improved versions, *Graf and Schulze* [1961]).
‡Tokyo surface ship vibrating string gravimeter [*Tomoda and Kanamori*, 1962].

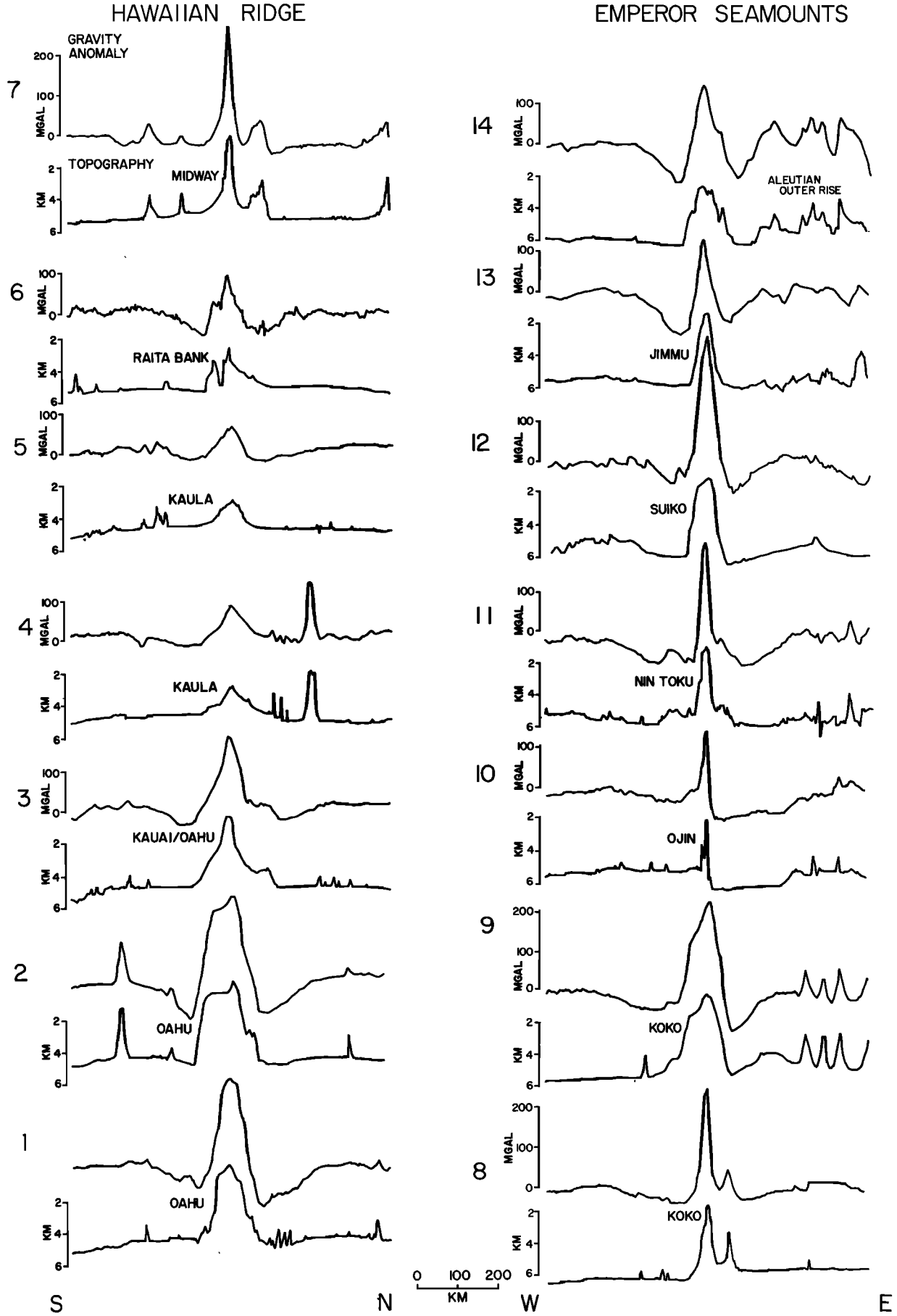

Fig. 2. Projected free air gravity anomaly and bathymetry profiles of the Hawaiian-Emperor seamount chain. Profile 1 is located near the southeastern end of the Hawaiian Ridge, and profile 14 near the northernmost end of the Emperor seamount chain (Figure 1).

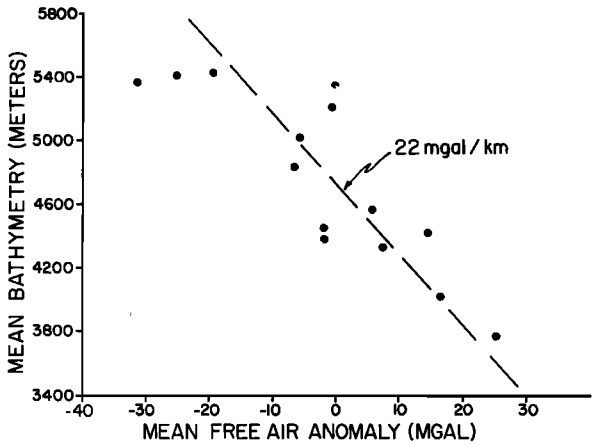

Fig. 3. Plot of mean free air gravity anomaly against bathymetry for profiles 1–14 (Figures 1 and 2). The dashed line indicates the 'best fit' line [from *Watts*, 1976], which explains the relationship between long-wavelength ($\lambda > 1600$ km) gravity anomalies and bathymetry over the southeastern end of the Hawaiian Ridge.

The required filter can then be obtained by inverse Fourier transforming the admittance.

In order to reduce the noise in the estimate of the admittance, however, some form of spectral smoothing is required. *McKenzie and Bowin* [1976] carried out ensemble averaging by subdividing their long profiles into a number of shorter profiles of equal length. They then averaged the spectra for each subprofile. The problem with this approach is that the subprofiles crossed a number of different geological features. Since a single feature is considered in this study, a different approach will be used. Specifically, many profiles over the same feature will be used, each of which constitutes an independent estimate of the relationship of gravity and bathymetry. The spectra are then averaged for each profile. By this procedure the filter or admittance is obtained for a single geological feature.

The basic computational steps are similar to those outlined by *McKenzie and Bowin* [1976]. Observed gravity and bathymetry profiles are linearly interpolated to obtain evenly spaced values. After the removal of the trend and mean the discrete Fourier transform is obtained by the use of the fast Fourier transform. The two transforms are used to estimate the cross spectrum and power spectrum and to construct an average over the set of profiles. In addition to determining the filter it is also useful to determine the coherence and the phase of the admittance [*McKenzie and Bowin*, 1976]. The coherence γ^2 is a measure of the portion of the gravity field which is caused by bathymetry. An estimate of the coherence is given by

$$\gamma^2 = (N(cc^*/E_G E_B) - 1)/(N - 1) \quad (5)$$

where $c = c(k_n)$ is the complex cross spectrum of gravity and bathymetry, E_G and E_B are the power spectra of gravity and bathymetry, respectively, and N is the total number of profiles. The phase of the admittance ϕ, defined by

$$\exp[-i2\phi(k_n)] = [Z(k_n)]/[Z^*(k_n)] \quad (6)$$

is important, since we expect that the filter coefficients of the earth filter is real and that the admittance $Z(k_n)$ is also real. The phase should therefore be close to zero.

The results of the computations are a filter or admittance which reproduces the gravity from the bathymetry over the feature which is being examined. The filter or admittance is based completely on the observed relationship between gravity and bathymetry and is not tied to any isostatic model. However, as was shown by *Lewis and Dorman* [1970], *Dorman and Lewis* [1970], *McKenzie and Bowin* [1976], *Walcott* [1976], and *Banks et al.* [1977], the filter or admittance can be easily compared with isostatic models based on different hypotheses of compensation.

DATA ANALYSIS

The method outlined in the previous section has been used to study the state of isostasy along the Hawaiian-Emperor seamount chain. A total of 14 projected bathymetry and free air gravity anomaly profiles of the chain were analyzed, each of which extended 400 km on either side of the crest of the seamount chain (Figures 1 and 2).

The mean and trend were removed from each bathymetry and gravity profile, and a cosine taper was applied before each time series was Fourier transformed. The trend removed was small, so the observed profiles in Figures 7 and 8 closely resemble those in Figure 2. The mean removed varied along the seamount chain (Figure 3). In general, the mean gravity anomaly is positive for mean depths shallower than 4.6 km

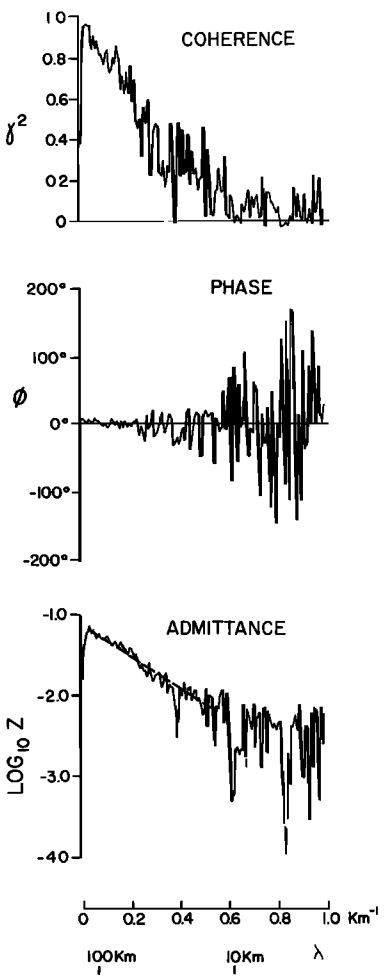

Fig. 4. The coherence, $\log_{10}$ of the amplitude of the admittance, and the phase in degrees of the admittance generated from the gravity and bathymetry profiles shown in Figures 1 and 2. The dashed line is a 'best fit' to the observed admittance for $10 < \lambda < 160$ km. The slope of this line gives an estimate of the mean water depth of 4.5 km, and the intercept of this line on the vertical axis gives an estimate of the uniform density contrast between sea floor topography and water of -1.77 g/cm^3.

TABLE 2. Spectral Estimates for $0.078 < k < 0.0313$

Wavelength, km^{-1}	Wavelength, km	Coherence γ^2	Phase ϕ	Sample admittance, mgal/km	Noise parameter σ^*	Standard error of admittance, † mgal/km	
						Minimum	Maximum
0.0078	805	0.357	6.2	16.1	0.253	12.8	21.5
0.0156	402	0.814	6.5	39.9	0.090	36.6	43.8
0.0235	267	0.956	1.3	58.2	0.041	55.9	60.7
0.0313	201	0.966	−0.3	60.1	0.036	58.0	62.3

*Here $\sigma = [(\gamma^{-2} - 1)/2p]^{1/2}$, where p is number of degrees of freedom [*Munk and Cartwright*, 1966]. In this study, p is number of gravity and bathymetry profiles.

†Obtained by assuming normal probability distribution of sample admittance/true admittance with standard error σ. This is approximately valid for $\sigma < 0.25$ [*Munk and Cartwright*, 1966, Figure 16). For higher σ the probability distribution is not normal and is positively biased.

and negative for greater depths (Figure 3). *Watts* [1976] obtained a 'best-fitting' slope of 22 mgal/km which described the relationship of 5 × 5° mean gravity and bathymetry over the Hawaiian swell. The general agreement between the mean values removed from the profiles and this best-fitting slope is evidence that relatively long wavelength features ($\lambda > 1600$ km) such as the Hawaiian swell have been removed from the observed profiles.

The resulting gravity and bathymetry profiles were used to obtain 14 independent estimates of the cross spectrum and power spectrum. The smoothed spectra were then used to compute the coherence γ^2, the phase of the admittance, and $\log_{10}$ of the amplitude of the admittance (Figure 4, Table 2). The relative smoothness of the $\log_{10}$ admittance plot for $0 < k < 0.55$ is evidence that the same signal was present in each profile and that the smoothing procedure satisfactorily reduces noise. The phase is approximately zero for these wave numbers, a situation implying the admittance is real. The coherence is high for $0.008 < k < 0.55$, indicating that a significant portion of the energy in gravity can be attributed to bathymetry.

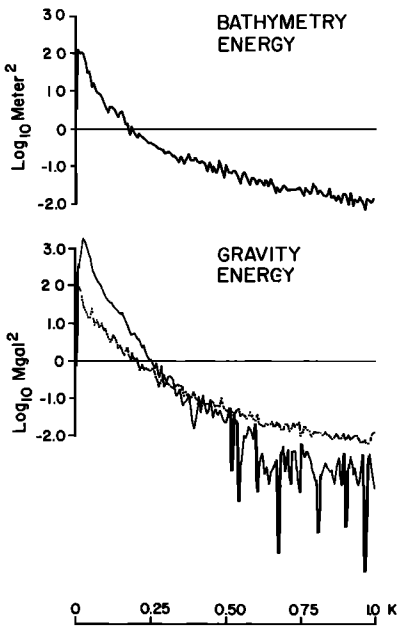

Fig. 5. The energy of the bathymetry and gravity generated from the gravity and bathymetry profiles in Figures 1 and 2. The upper diagram shows the energy of the bathymetry relative to 2.2×10^7 m². The lower diagram shows the energy of the gravity relative to 1.4×10^4 mgal². The solid curve in this diagram indicates the height of the energy coherent with the bathymetry, and the dotted curve indicates the height of the energy incoherent with the bathymetry. This diagram shows that incoherent energy contributes a small fraction to the total energy for $0 \leq k \leq 0.26$ and a large fraction to the total energy for $0.5 \leq k \leq 1.0$.

The energy in the gravity and bathymetry is shown in Figure 5. The peak in the bathymetry at $k \sim 0.0235$ ($\lambda \sim 265$ km) corresponds to wavelengths represented by individual seamounts along the chain. The gravity energy has been divided into a coherent and an incoherent part. The coherent energy is a measure of the energy in the gravity field which is caused by topography. The incoherent energy is a measure of the energy due to other effects, such as instrument noise and non-two dimensionality. For $k < \sim 0.3$ ($\lambda > \sim 10$ km) the coherent energy is dominant, but for $k > \sim 0.3$ the incoherent energy dominates.

The filter shown in Figure 6 was obtained by inverse Fourier transforming the admittance. The filter can be considered an impulse response function representing the gravity effect of a line load. The broad negative lobes of the filter therefore represent the effect of isostatic compensation. The extent to which the filter (Figure 6) can reproduce observed gravity anomalies is shown in Figures 7 and 8. The filtered topography profiles in these figures were obtained by inverse Fourier transforming the product of the observed admittance and the fourier transform of the observed bathymetry. This operation, which is carried out in the frequency domain, is equivalent to convolving the observed filter (Figure 6) with the observed

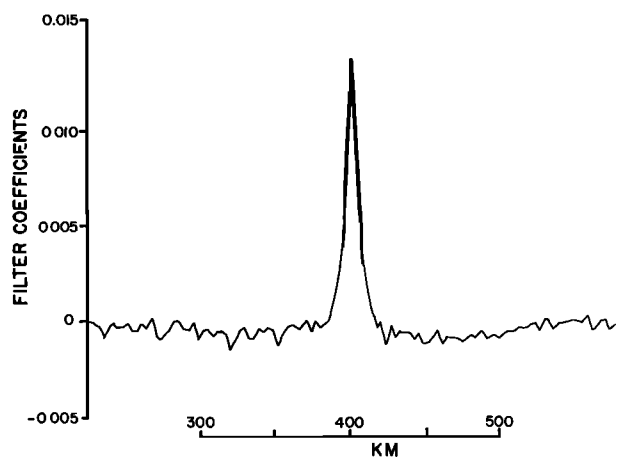

Fig. 6. The filter generated from the gravity and bathymetry profiles in Figures 1 and 2. The filter shows well-developed side lobes. The total filter length is 800 km, and only part of the filter, between 250 and 550 km, is shown here.

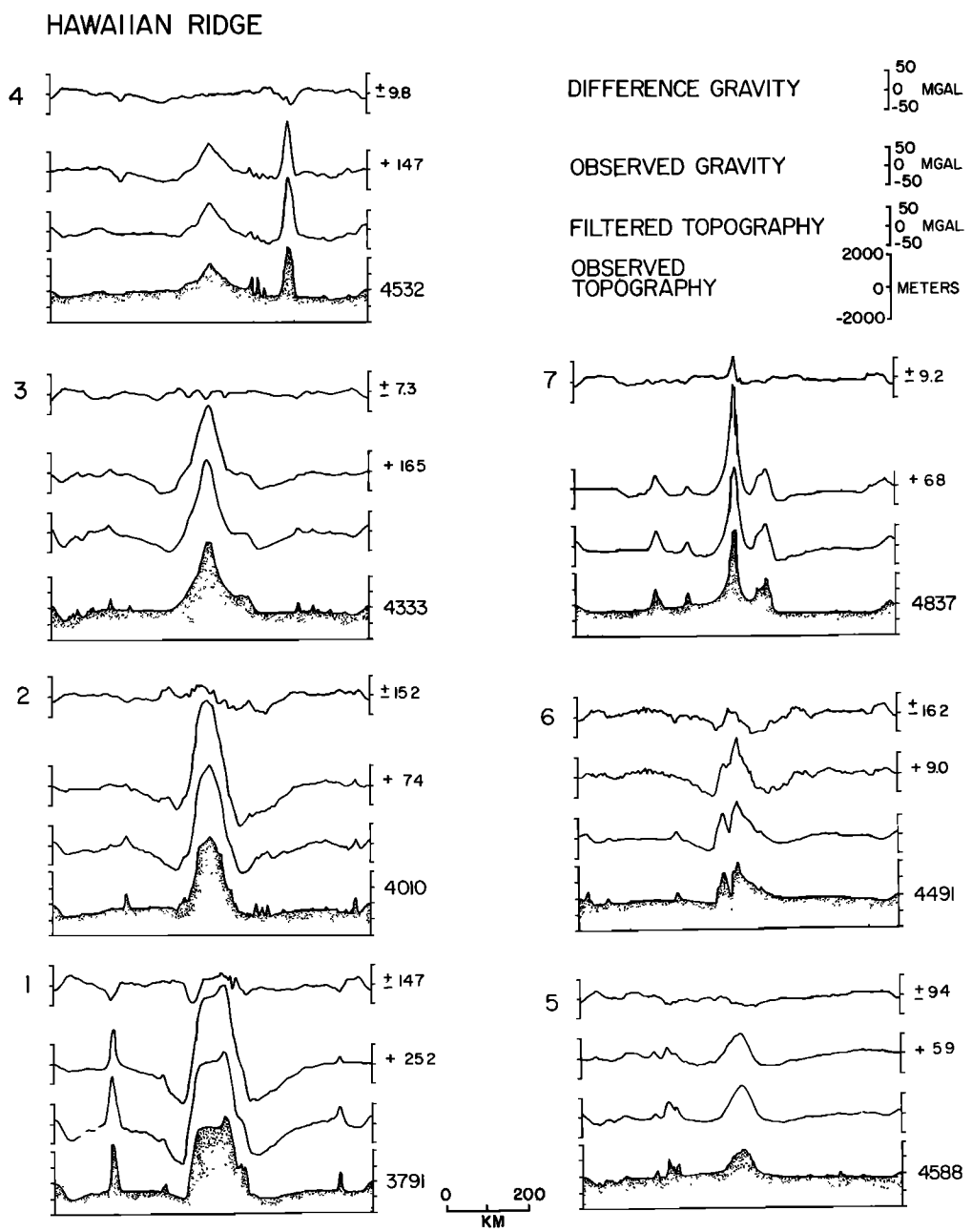

Fig. 7. Difference gravity, observed gravity, filtered bathymetry, and observed bathymetry profiles 1–7 of the Hawaiian Ridge. The observed gravity and bathymetry profiles are the observed profiles in Figure 2 with their mean and trend removed. The mean removed is indicated to the right of each profile. These profiles closely resemble those in Figure 2, since the trend removed is negligible. The filtered topography profiles were obtained by inverse Fourier transforming the product of the observed admittance and the Fourier transform of the bathymetry. This operation, which is carried out in the frequency domain, is equivalent to convolving the observed filter (Figure 6) with the observed bathymetry. The difference gravity profile is the difference between observed gravity and filtered bathymetry and represents that part of the gravity field which cannot be explained by the filter.

bathymetry. The filtered topography profiles (Figures 7 and 8) generally compare well with the observed gravity anomaly profiles. The main differences are for short-wavelength bathymetry features on either side of the seamount chain and over the crest of the chain. The standard deviation between these predicted and observed anomalies is better than ± 15 mgal for 66% of the profiles.

INTERPRETATION

The simplest model for explaining the observed admittance values is to assume that the gravity anomalies are due only to the sea floor topography and that the topography is uncompensated. The admittance expressing the relationship of gravity to uncompensated topography is given [*Walcott*, 1976; *McKenzie and Bowin*, 1976] by

$$Z(k_n) = 2\pi G(\rho_2 - 1.03) \exp -k_n d \qquad (7)$$

where ρ_2 is the density of the topography and d is the mean water depth. This expression is the first term in the Fourier transform of the gravity effect of a sinusoidal density layer at a water depth d.

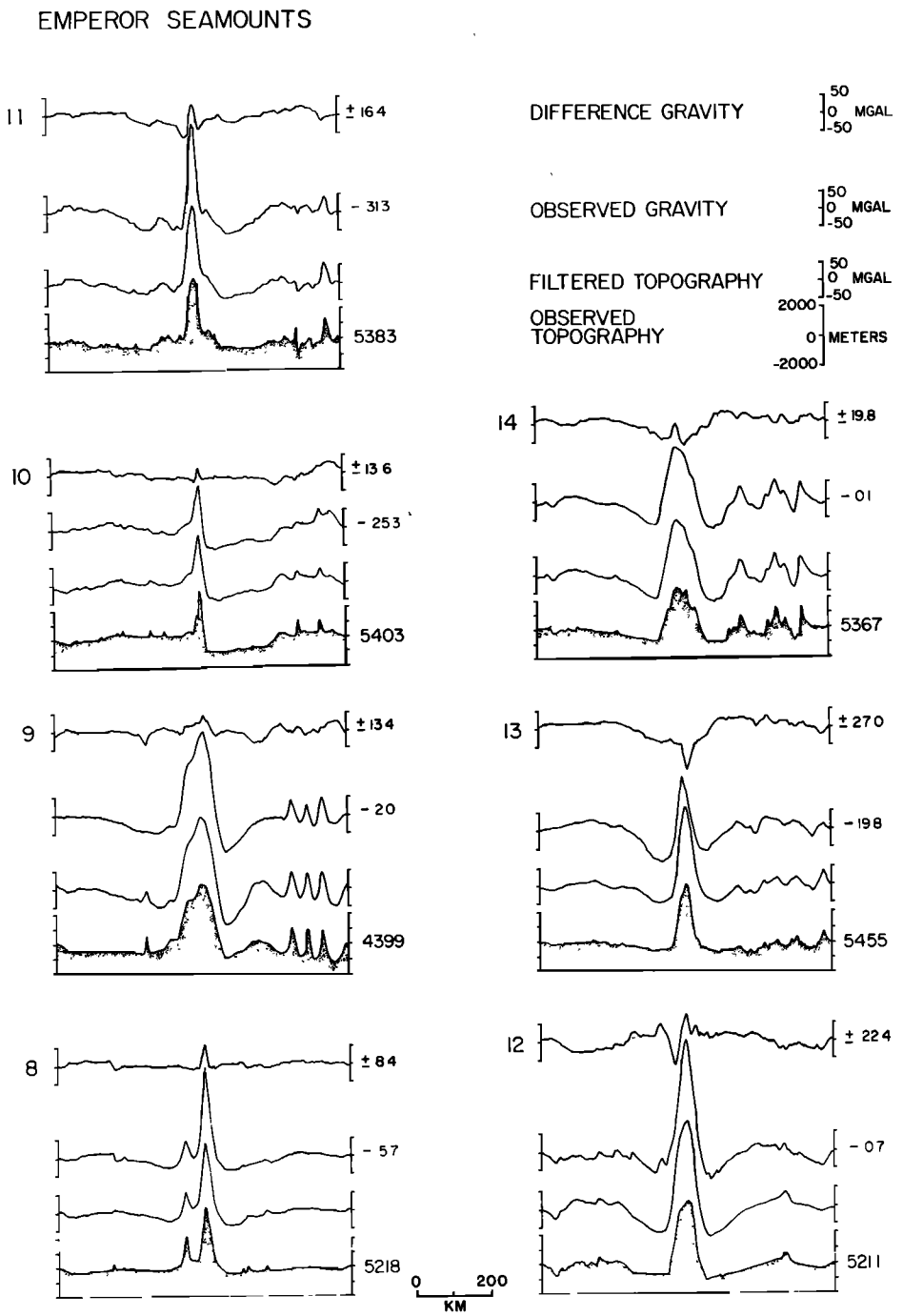

Fig. 8. Difference gravity, observed gravity, filtered bathymetry, and observed bathymetry profiles 8–14 of the Emperor Seamounts. The legend is the same as that for Figure 7.

Equation (7) gives a straight line on a $\log_{10}$ admittance against wave number k_n plot, and thus estimates of ρ_2 and d can be made [*McKenzie and Bowin*, 1976]. The slope of the line is given by $0.4335d$ and the intercept by $\log_{10}(2\pi G(\rho_2 - 1.03))$. A best fit straight line for the admittance for $0.03 < k_n < 0.30$ gave estimates of $d = 4.5$ km and $\rho_2 = 2.8$ g cm^{-3}. The straight line is shown in Figure 4. Although there is some scatter, this line explains the data reasonably well. The estimate of d is slightly smaller than the observed mean water depth but is within the range of observed values (Figure 3). By accepting this value an estimate for the density of the topography of 2.8 g cm^{-3} is obtained. This is somewhat higher than the value of 2.3 g cm^{-3} assumed by *Woollard* [1951] for Oahu but is similar to the values deduced by *Robertson* [1967, 1970] from density measurements on the Cook Islands.

Although the short wavelength ($20 < \lambda < 200$ km) portion of the $\log_{10} Z$ curve can be well fit by a straight line, the admittance decreases rapidly at longer wavelengths because of the effects of isostasy. As a compensated topographic feature becomes wider, the gravity anomalies over its center decrease and the patterns of gravity and bathymetry become less similar. The nature of the relationship between gravity and bathymetry for various theoretical isostatic models can be determined [*Walcott*, 1976; *McKenzie and Bowin*, 1976] and compared to observed values. However, only models in which the deflection is symmetric about a line load can be easily

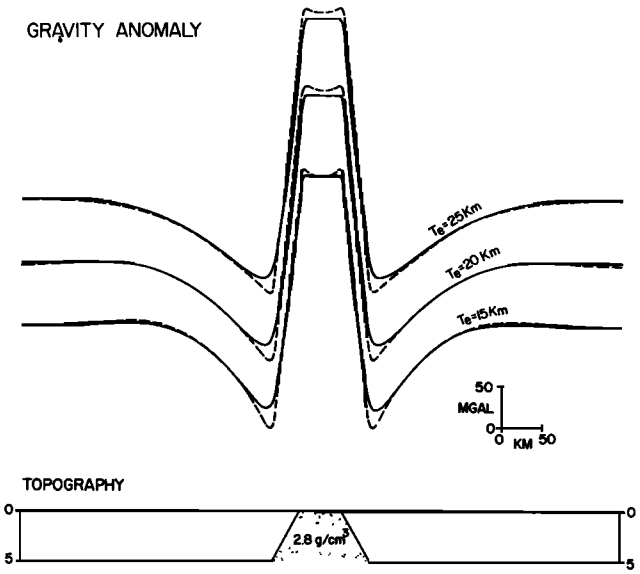

Fig. 9. Comparison of the gravity effect of the simple model of flexure computed by using the line integral method and the Fourier method. The gravity effect has been computed for a range of values of elastic thickness typical of the Hawaiian Ridge and Emperor Seamounts (Figure 11). The largest discrepancies occur over the crest of the seamount and over flanking regions.

considered. This limitation is not restrictive, since both the Airy model and the continuous plate model [*Walcott*, 1970*a*; *Watts and Cochran*, 1974] can be examined.

The admittance for the simple Airy model of compensation is given by the sum of the Fourier transforms of two sinusoidal density layers, one at the mean water depth, giving the topography, and one at the depth of compensation, representing the compensation [*McKenzie and Bowin*, 1976]. The resulting expression is

$$Z(k_n) = 2\pi G(\rho_2 - 1.03)(\exp - k_n d)(1 - \exp - k_n t) \quad (8)$$

where t is the distance below the sea floor at which compensation is assumed to occur. For simple Airy isostasy, t is approximately the average crustal thickness. The other parameters are as given in (7).

A similar procedure is used to determine an expression for the admittance when a elastic plate model of compensation is assumed, although the computations are more involved, since the deflection due to the load must be calculated as part of the computation of the gravity effect of the compensation. *McKenzie and Bowin* [1976] outline a procedure for the derivation. The expression which we use for the admittance, $Z(k_n)$, differs slightly from that given by *McKenzie and Bowin* [1976]. The expression which they use (their equation (A16)) assumes that the entire crust has the same density as the topographic relief. Since the oceanic crust is 'layered,' another density contrast is introduced within the crust which corresponds to the layer 2/layer 3 transition. The resulting admittance is then

$$Z(k_n) = 2\pi G(\rho_2 - 1.03)(\exp - k_n d)\{1 - [(\exp - k_n t_2)(\rho_3 - \rho_2) + (\exp - k_n t_c)(\rho_m - \rho_3)]/((\rho_m - \rho_2) + 4(\rho_m - 1.03)Mk'^2AB^{-1})\} \quad (9)$$

where t_2 is the thickness of layer 2; t_c is the mean thickness of the crust; ρ_3 is the density of layer 3; ρ_m is the density of the upper mantle; $M = E/3gh(\rho_m - 1.03)$, where E is Young's modulus and the plate thickness is $2h$; $k' = kh$; $A = [(\sinh 2k')/2k']^2 - 1$; and $B = [(\sinh 4k')/4k']^2 + 1$.

The method used to compute the gravity effect of these models is approximate, since only the first term in the Fourier

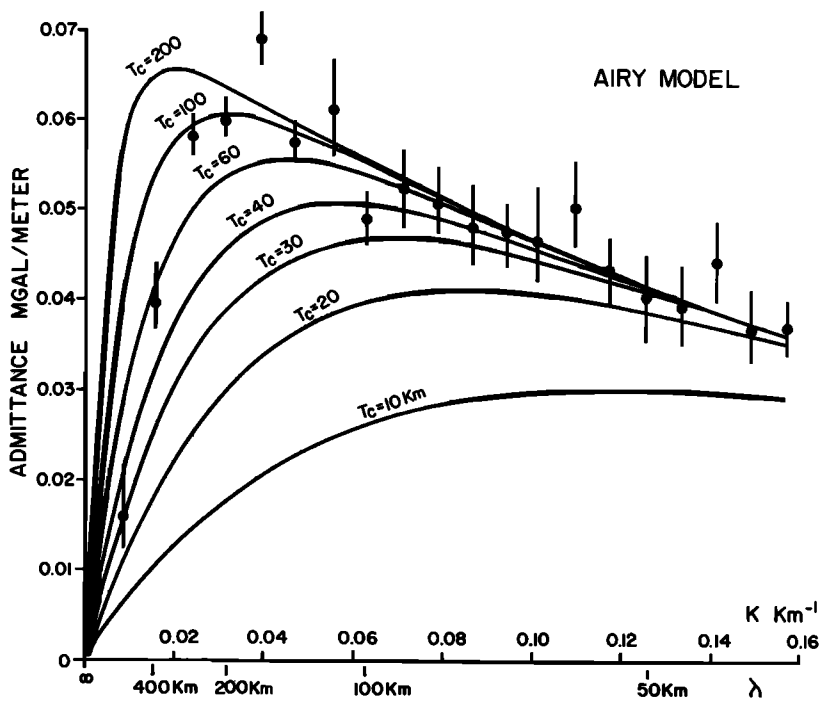

Fig. 10. Observed admittance values (solid circles) generated from gravity and bathymetry profiles in Figures 1 and 2 of the Hawaiian-Emperor seamount chain. The standard error on each estimate is computed from the coherence, a normal probability distribution for the ratio of the true/sample admittance being assumed. The solid curves indicate theoretical models based on the Airy model of isostasy. The theoretical models are based on the parameters summarized in Table 3 and the assumed values of the crustal thickness T_c shown. A mean water depth of 4.5 km and a uniform density contrast of -1.77 g cm^{-3} between water and sea floor topography are assumed.

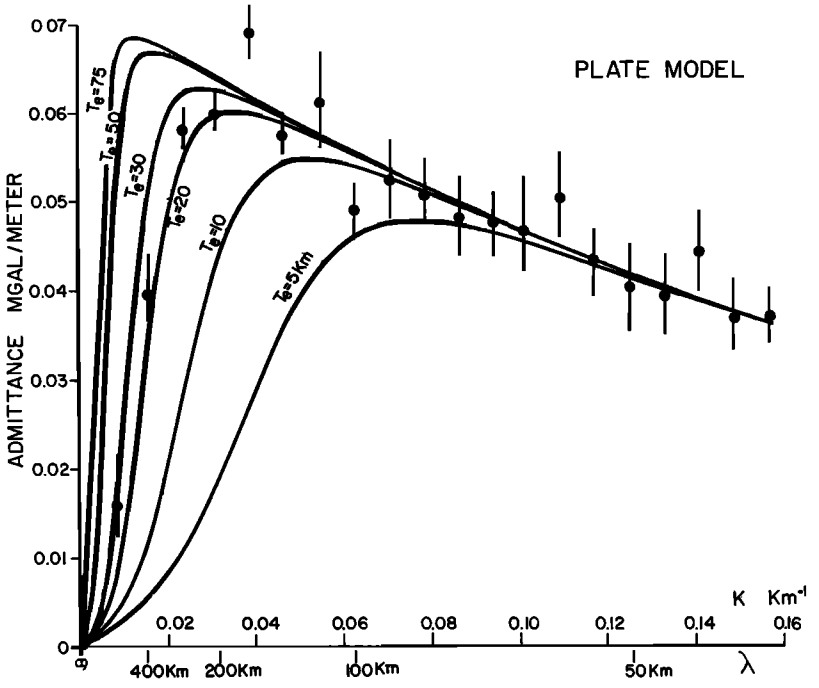

Fig. 11. Observed admittance values (solid circles) compared with theoretical models based on the plate model of isostasy. The parameters assumed are the same as those in Figure 10.

series expansion for the gravity effect is used (for example, *Parker* [1972]). The Fourier method compares well, however, to a line-integral method of computing the gravity effect for the theoretical seamount load in Figure 9. The differences between the methods are small and occur mainly on the crest and flanks of the seamount.

The calculated admittance curves for the Airy and plate models of compensation are compared with observed values in Figures 10 and 11. The parameters assumed in the computations are summarized as follows:

t_2 thickness of Layer 2, equal to 1.5 km;
t_c mean thickness of oceanic crust, equal to 5 km;
ρ_m density of mantle, equal to 3.4 g cm^{-3};
ρ_3 density of layer 3, equal to 2.9 g cm^{-3};
ρ_2 density of topography, equal to 2.8 g cm^{-3};
d mean water depth, equal to 4.5 km;
E Young's modulus, equal to 10^{12} dyn cm^{-2}.

For short wavelengths ($\lambda < 100$ km) the curves for both models asymptotically approach a line representing uncompensated topography. The models differ significantly for long wavelengths ($\lambda > 100$ km). The computed curves for the Airy model (Figure 10) fit the long-wavelength admittance values poorly. The best-fitting average crustal thicknesses are in the range 30–90 km. These thicknesses are much greater than the maximum thickness of crust deduced from seismic refraction studies along the seamount chain (for example, *Shor* [1960], *Furumoto and Woollard* [1965]), suggesting that the Airy model is not a realistic isostatic model for the seamount chain. In contrast, the computed curves for the plate model (Figure 11) fit the long-wavelength values well. The best-fitting estimate for the elastic thickness of the oceanic lithosphere is in the range 20–30 km. These estimates are similar to previous values determined for the interior of the oceanic lithosphere by *Walcott* [1970*a*], *Watts and Cochran* [1974], and *Watts et al.* [1975].

The observed admittance values (Figures 10 and 11) only contain information on the overall state of isostasy along the seamount chain. The state of isostasy may, however, change along the chain, since both the age of individual seamounts [*Dalrymple et al.*, 1974; *Clague and Jarrard*, 1973] and the inferred age of the oceanic crust underlying the seamounts varies along the chain. Any changes in isostasy along the chain have been smoothed out by the averaging process.

To evaluate whether or not the elastic thickness changes along the chain, computed gravity anomalies were generated for different values of the elastic plate thickness. The best-fitting plate thickness was determined as that value which minimized the sums of the squares of residuals between computed and observed gravity anomalies. A similar approach was used by *Watts and Cochran* [1974] except that they did not use the fast Fourier transform. A uniform density of 2.8 cm^{-3} was assumed for the sea floor topography on each profile, which is the same as that determined from spectral analysis of all the profiles (Figure 4).

The procedure used is illustrated for profiles of the Hawaiian Ridge and Emperor Seamounts in Figures 12 and 13. Figures 12 and 13 show the computed gravity anomalies for different assumed values of the elastic thickness as well as the difference gravity anomalies. The difference anomalies were obtained by subtracting the observed anomalies from the computed anomalies, based on the theoretical filters. These anomalies therefore represent regional isostatic anomalies [*Vening Meinesz*, 1941]. The best-fitting plate thickness can therefore be estimated as that value which best reduces these anomalies.

Table 3 summarizes the results of these computations for all profiles of the seamount chain. The range of values for the best fit elastic thickness is 13–36 km, and the mean and standard error of all the determinations is 25 ± 9 km. These estimates are very similar to those obtained from spectral analysis of all the profiles (Figures 10 and 11). The main difference is the increased scatter due to the difficulty of choosing a minimum for some profiles and because amplitude rather than wavelength is emphasized in selecting the best fit.

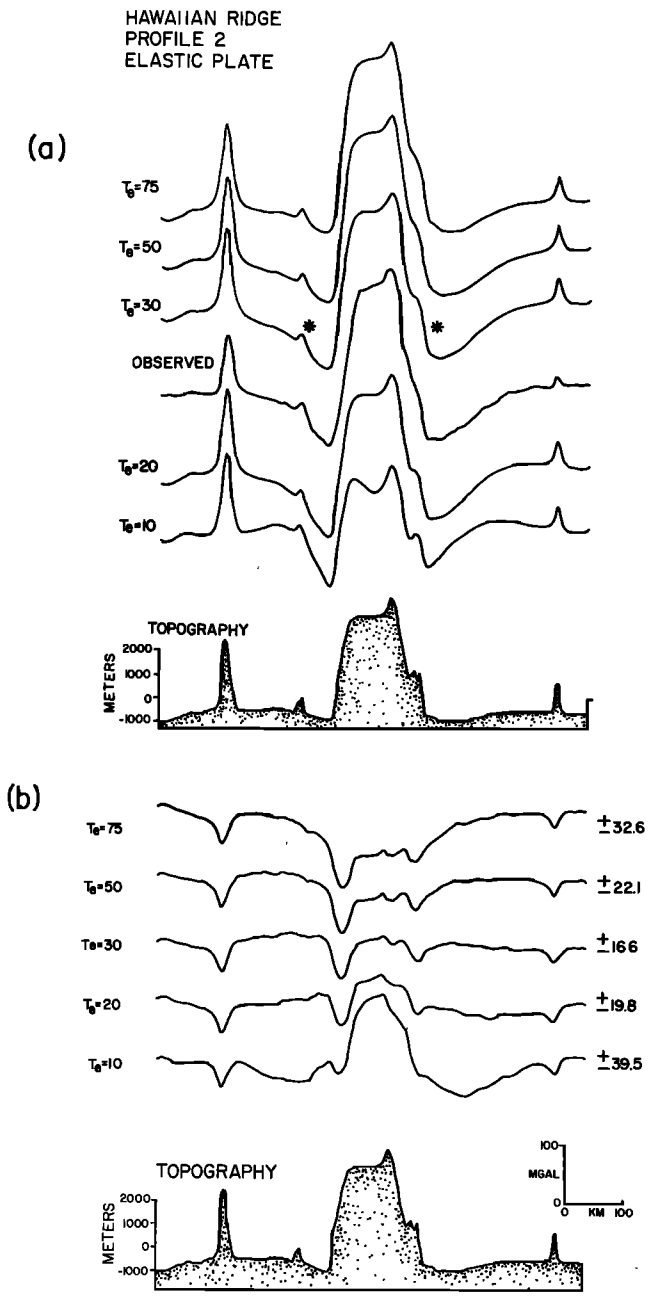

Fig. 12. (*a*) Observed gravity and bathymetry profile 2 of the Hawaiian Ridge compared with theoretical profiles generated for elastic plate thicknesses of 10, 20, 30, 50, and 75 km. The theoretical profile for T_e = 30 km most closely resembles the wavelength and amplitude of the observed profile. Asterisks indicate portions of the theoretical profile which explain 'observed' data particularly well. (*b*) Difference gravity profiles obtained by subtracting theoretical from 'observed' profiles for elastic plate thicknesses of 10, 20, 30, 50, and 75 km. These profiles represent regional isostatic anomaly profiles. The smallest rms difference between observed and theoretical profiles is for a plate thickness of T_e = 30 km.

The results in Table 3 show that the Hawaiian Ridge is associated with plate thicknesses in the range 17–37 km and the Emperor Seamounts are associated with thicknesses in the range 10–36 km. Relatively low values of 10–20 km occur for the three northernmost profiles of the Emperor Seamounts, and relatively high values of 17–37 km occur for the Hawaiian Ridge and the three southernmost profiles of the Emperor Seamounts.

An independent test of these estimates is to compare the associated crustal flexure with seismic evidence of the configuration of individual crustal layers beneath the seamount chain. Unfortunately, only limited seismic data are available along the chain (for example, *Shor* [1960], *Furumoto and Woollard* [1965], *Den et al.* [1969], *Houtz* [1976]). The only determinations of the 'Moho' are at French Frigate Schoals and near Oahu. Although there is some uncertainty, the depth to Moho is about 22 km beneath Oahu [*Furumoto and Woollard*, 1965]. As was pointed out by *Walcott* [1970*a*], this does not fit the plate model, unless a model in which the lithosphere is fractured beneath the seamount during loading is used. The depth to Moho beneath French Frigate Shoals is about 15 km [*Shor*, 1960], and this is more easily explained by the plate model.

Woollard [1966] argued that the seismic data do not support flexure models because of thickening of the high-velocity basal crustal layer 3 beneath Oahu. However, *Watts et al.* [1976] suggested that this might result from the fact that Hawaiian basaltic magma tends to form dense nonvesicular rocks with densities of 2.9–3.0 g cm^{-3} when it is erupted at depths greater than about 1 km. If a majority of the Hawaiian Ridge basalts were erupted at depth, they could have densities similar to

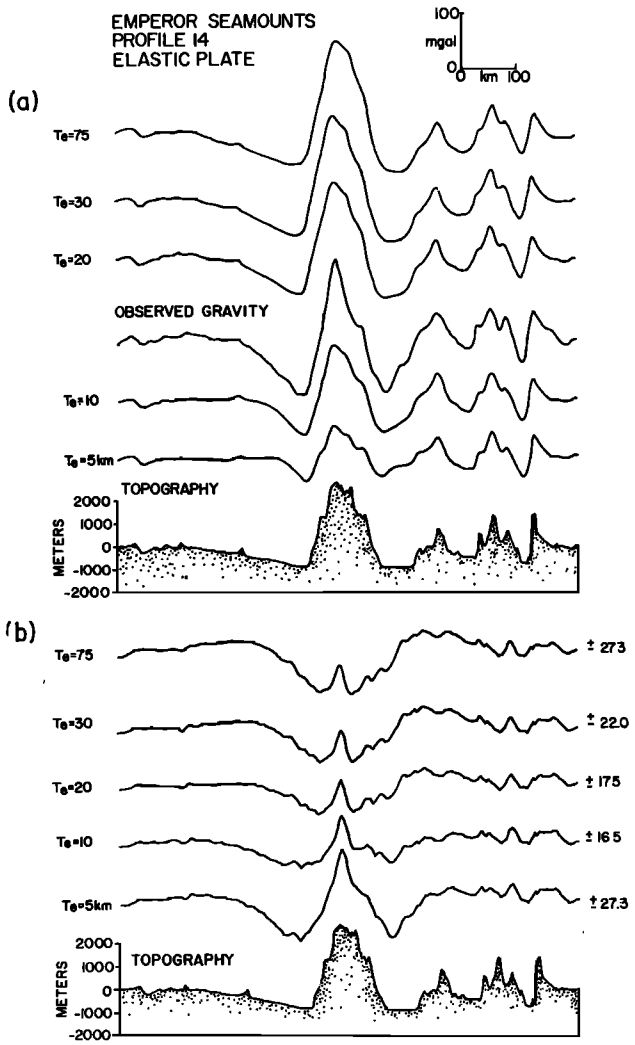

Fig. 13. (*a*) Observed gravity and bathymetry profile 14 of the Emperor Seamounts compared with theoretical profiles generated for elastic plate thicknesses of 5, 10, 20, 30, and 75 km. The theoretical profiles for T_e = 10 km most satisfactorily explain the amplitude and wavelength of the 'observed' profile. (*b*) Difference gravity profiles. The smallest rms difference is for a plate thickness of T_e = 10 km.

TABLE 3. Estimated Age of Crust at Time of Loading and 'Best Fit' Elastic Thickness of the Oceanic Lithosphere

Profile	Estimated age of load,* m.y. B.P.	Estimated age of crust,† m.y. B.P.	Estimated age of crust at time of loading, m.y. B.P.	'Best fit' elastic thickness, km
		Hawaiian Ridge		
1	3	80	77	30
2	3	80	77	32
3	5	80	75	30
4	7.5	80	72.5	30
5	7.5	80	72.5	20
6	13	96	83	17.5
7	18	105	87	37
		Emperor Seamounts		
8	44	115	71	30.5
9	48.5	115	66.5	36
10	48.5	100	51.5	no estimate
11	52	80‡	28	20
12	55	80‡	25	no estimate
13	56	80‡	24	10.5
14	58.5	80‡	22.5	13

*Based on the work of *Clague and Jarrard* [1973].
†Based on magnetic anomaly identifications and tectonic reconstructions in *Hilde* [1973].
‡Assumes a model in which the crust under the northernmost seamounts is Late Cretaceous and that the Emperor trough is a fracture zone offset.

those of oceanic layer 3. In the plate model it is assumed that the basalt constitutes a load on the oceanic crust, since it displaces sea water. If basalt is being intruded at depth, it will contribute to the load and cause an additional deflection.

Radiometric age dating of rock samples from outcrops and dredge hauls suggests that the age of individual seamounts progressively increases along the seamount chain (for example, *Clague and Jarrard* [1973], *Dalrymple et al.* [1974]). The low values of the elastic thickness obtained for the Emperor Seamounts north of 40°N (Table 3) may therefore be caused by a viscous reaction of the lithosphere to the load of the seamount chain through time.

We can examine this possibility by using a simple viscoelastic (Maxwell) plate model similar to that used previously by *Walcott* [1970*b*] and *Watts and Cochran* [1974]. This model is somewhat limited in its applicability to the lithosphere. The main problem is that it assumes uniform viscosity. More complex models in which viscosity varies as a function of temperature (depth) have not been examined.

The viscoelastic (Maxwell) plate model requires knowledge of the original thickness of the lithosphere at the onset of loading. We will assume that this thickness corresponds to the short-term seismic thickness of the lithosphere. The seismic thickness can be estimated if the age of the lithosphere at the onset of loading is known [*Forsyth*, 1977]. Therefore the main problem is to estimate the age of the seamount and the age of the underlying oceanic crust.

Even though the age of seamounts along the chain are comparatively well known (for example, *Clague and Jarrard* [1973]), the age of the underlying crust is poorly known. Magnetic lineations which can be correlated with the geomagnetic time scale have been mapped at only a few locations along the chain [*Hilde*, 1973]. However, a number of tectonic reconstructions have been made based on these lineations and other lineation patterns in the north Pacific which allow a reasonably good estimate of the age of the crust underlying the chain to be made.

The tectonic reconstruction of the northwest Pacific by *Hilde* [1973] shows a magnetic bight between the Shatsky rise and the junction of the Kuril and Aleutian trenches. This bight connects the northeast-southwest trending Japanese lineations [*Larson and Pitman*, 1972] with the east-west trending lineations south of the Aleutian trench [*Grow and Atwater*, 1970]. Therefore the Hawaiian Ridge trends nearly parallel to the inferred isochrons, while the Emperor Seamounts cross them at a high angle. Thus the age of the crust beneath the northern most Emperor Seamounts is generally similar to that beneath the southeastern end of the Hawaiian Ridge, reaching a minimum of about 80 m.y. or 65 m.y. depending on the tectonic significance of the Emperor Trough.

For purposes of the computations the mean age of the crust assumed beneath the Emperor Seamounts and the Hawaiian Ridge was 100 and 80 m.y. B.P., respectively. Based on the ages of the seamount chain by *Clague and Jarrard* [1973], these ages imply an average for the age of the lithosphere at the time of loading of about 50 and 70 m.y.

The transfer function was computed for the Emperor Seamounts and Hawaiian Ridge and compared with theoretical curves based on the viscoelastic model (Figure 14). Relatively smooth values of the transfer function were obtained even though spectra were averaged over only 7 profiles. The value of T_0, the original thickness of the lithosphere, was based on an estimate of the average age of the lithosphere at the time of loading and the relationship between age and lithospheric thickness given by *Forsyth* [1977].

Figure 14 shows that the transfer function along the Emperor Seamounts and Hawaiian Ridge can be explained by a viscoelastic model with a relaxation time constant in the range 10^5–10^7 years. The Hawaiian Ridge is explained by relatively low values of 10^5–10^6 years, and the Emperor Seamounts by higher values of 10^6–10^7 years. These results suggest significant variations in the time constant along the chain. For example, the value of 10^5 years proposed by *Walcott* [1970*b*] for the lithosphere explains the Hawaiian Ridge but cannot explain

the Emperor Seamount data. In a similar way the values suggested by *Watts and Cochran* [1974] of $>10^7$ years can explain the Emperor Seamounts but cannot explain the Hawaiian Ridge data.

These large differences in the relaxation time constant (10^6–10^7 years) suggest that a viscoelastic plate model cannot satisfactorily explain the observed differences in the elastic thickness along the seamount chain. An alternative explanation to these observations is for an elastic model in which the elastic thickness is acquired at the time of loading and does not change appreciably with time.

This possibility can be tested by examining the relationship between elastic thickness and age of the crust at the time of loading along individual gravity and bathymetry profiles of the seamount chain. The age of the crust at the time of loading inferred from age data along the chain [*Clague and Jarrard,* 1973] and from the tectonic reconstruction of the northwest Pacific by *Hilde* [1973] reaches a minimum of 22.5 m.y. for profile 14 of the northern Emperor Seamounts and a maximum of 87 m.y. for profile 7 of the Hawaiian Ridge (Table 3). Table 3 shows that the relatively low values of the elastic thickness determined along the seamount chain (10–20 km) correspond to young crust at the time of loading (22.5–28 m.y.) and that the relatively high values (17–37 km) correspond to old crust (66.5–87 m.y.). Thus a simple relationship may exist between elastic thickness and the age of the crust at the time of loading.

There have been two previous studies of surface loads on other parts of the Pacific oceanic plate which also provide information on the relationship between elastic thickness and crustal age. *McAdoo et al.* [1978] estimated the elastic thickness of the Pacific plate from the amplitude and wavelength of the Outer Rise seaward of the Kuril Trench. Evidence from magnetic lineations [*Hilde,* 1973] suggest that the age of the plate is 110–115 m.y. *McAdoo et al.* [1978], on the basis of 12 profiles of the Outer Rise, estimated the elastic thickness in the range of 25–47 km. *Cochran and Watts* [1978] estimated the elastic thickness associated with the topography of oceanic layer 2 at the East Pacific rise crest. They used cross-spectral techniques on 24 gravity and bathymetry profiles of the rise crest. Each profile extended 150 km on either side of the ridge axis and therefore crossed crust of 0–3 m.y. *Cochran and Watts* [1978] estimated the elastic thickness at the ridge axis to be in the range 2–6 km.

The elastic thickness for the Hawaiian-Emperor seamount chain, Kuril Outer Rise and East Pacific rise crest are plotted against inferred age of the crust at the time of loading in Figure 15. This figure shows that there is a simple relationship between elastic thickness and crustal age. Surface loads associated with young lithosphere (<25 m.y.) are supported by an elastic plate 2 to 20 km thick, and loads an old lithosphere (25–115 m.y.) are supported by a plate 20 to 45 km thick. There is apparently (Figure 15) an exponential increase in the elastic thickness with increase in crustal age. This suggests that the elastic thickness is related to the temperature gradient of the lithosphere at the time of loading.

Figure 15 shows that the elastic thickness estimates determined from different surface loads on the Pacific plate can be reasonably well fit by the 450 ± 150°C oceanic isotherm, based on simple thermal models for the cooling lithosphere. Thus the low values for the elastic thickness (2–6 km) determined at the East Pacific rise crest [*Cochran and Watts,* 1978] can be explained if the axial region of the rise crest is relatively thin and hot, and the high values (25–47 km) determined at the Kuril Outer Rise [*McAdoo et al.,* 1978] can be explained if the approaching Pacific plate is relatively thick and cold. Figure 15 suggests that at temperatures less than 450 ± 150°C the Pacific lithosphere responds elastically on long time scales and that at higher temperatures the lithosphere probably deforms plastically.

The elastic thickness estimates determined along the seamount chain are in good agreement with the simple thermal model (Figure 15). Since the age of individual seamounts increases by about 56 m.y. along the chain, there is therefore good evidence that the elastic thickness is acquired at the time of loading and does not change appreciably with time. This conclusion supports an earlier suggestion by *Watts and Cochran* [1974] that the oceanic lithosphere is elastic rather than viscoelastic on long time scales.

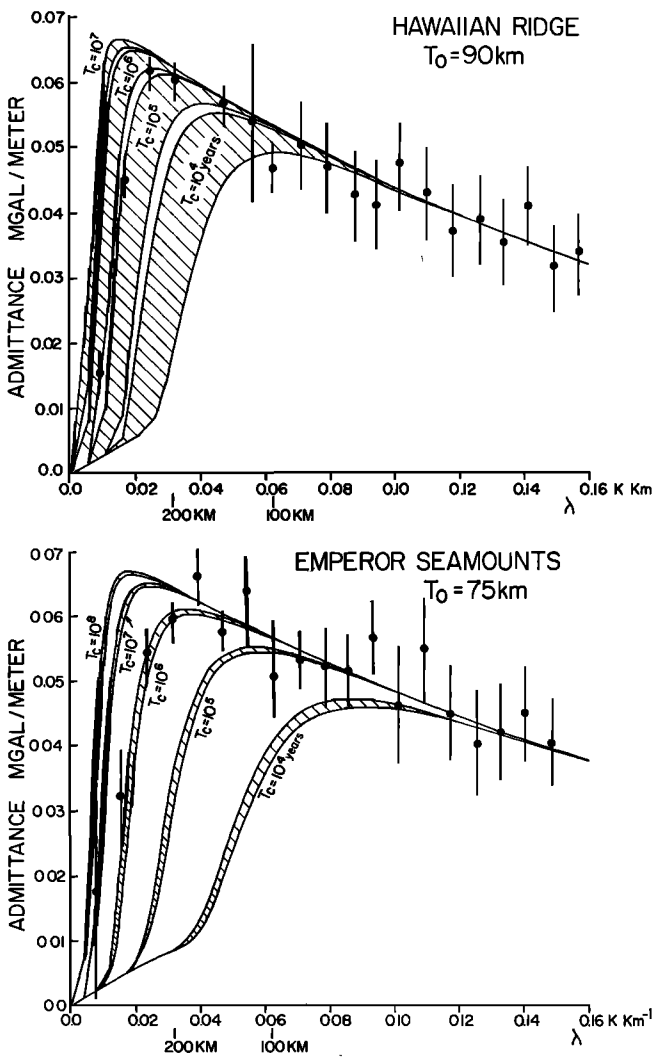

Fig. 14. Observed admittance values for the Hawaiian Ridge and Emperor Seamounts compared with theoretical models based on a viscoelastic (Maxwell) plate. The theoretical models are based on different values of the viscoelastic relaxation time constant T_c. The range in the models (shown by diagonal shading) reflects differences in the age of individual seamounts along the chain. The Hawaiian Ridge models are computed for an assumed value of T_0 = 90 km (see text for explanation), a mean water depth of 4.8 km, a uniform density contrast of -1.77 g cm^{-3}, and other parameters summarized in Table 3. The Emperor Seamount models are computed for an assumed value of T_0 = 75 km, a mean water depth of 4.2 km, and a uniform density contrast of -1.77 g cm^{-3}. The mean water depths and uniform density contrasts were deduced from the 'best fit' line for $10 < \lambda < 160$ km.

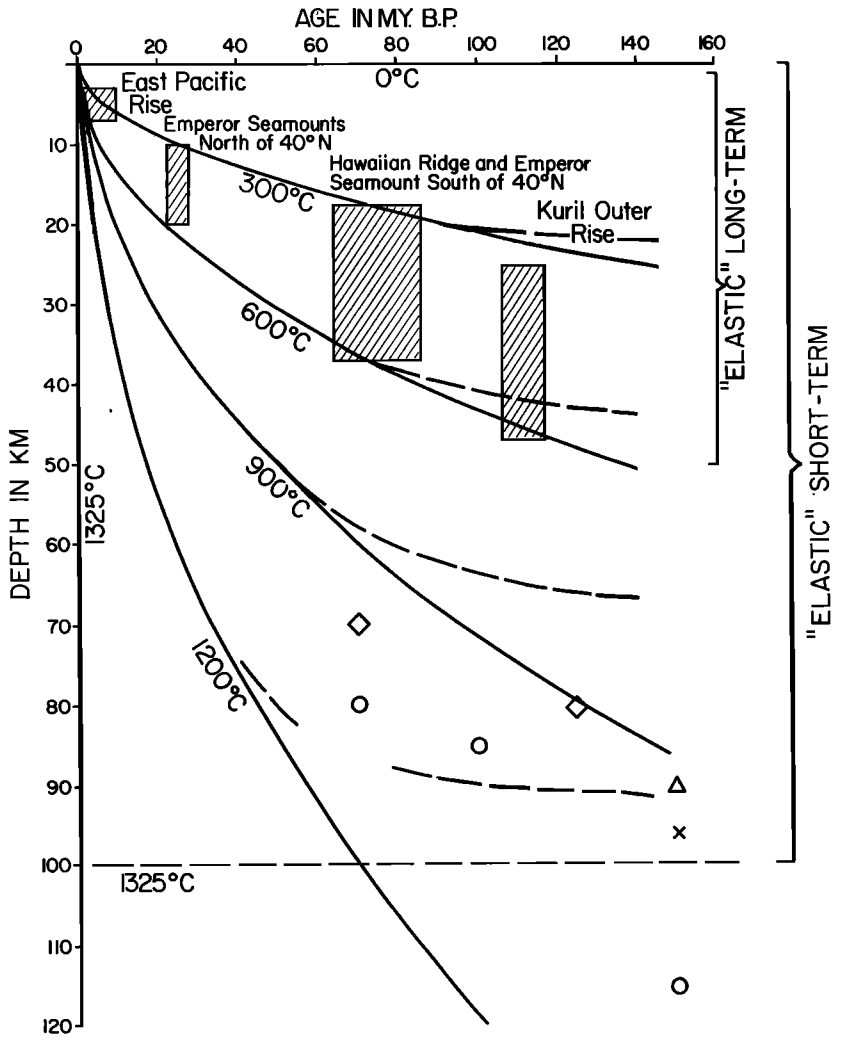

Fig. 15. Plot of isotherms for a simple cooling half-space model (solid curves) and plate model (dashed curves) [*Parsons and Sclater*, 1977]. The assumed initial temperature is 1325°C, the heat capacity is 0.3 kcal g^{-1} $°C^{-1}$, and the thermal conductivity is 7.5 × 10^{-3} kcal $°C^{-1}$ cm^{-1} s^{-1}. Lithospheric thickness estimates were deduced from short-period (20–200 s) Rayleigh wave dispersion data summarized in *Forsyth* [1977]. Also shown are elastic thickness estimates deduced from long-period (> 10^6 years) surface loads by *Cochran and Watts* [1978] for the East Pacific Rise, by *McAdoo et al.* [1978] for the Kuril Outer Rise, and in Table 3 for Hawaiian-Emperor seamount chain.

DISCUSSION

We have used gravity and bathymetry data along the Hawaiian-Emperor seamount chain to establish that the elastic thickness of the Pacific oceanic lithosphere depends on crustal age and hence temperature and that it does not change appreciably with time. This result is not in conflict with thermal models which predict that the lithosphere thickens and cools with time. Although the depth to the 450°C isotherm, for example, increases through time, the cooled lithosphere which is added has not been deformed by the surface load, and the elastic thickness acquired at the time of loading is not altered. The lithosphere would, however, deform in response to subsequent loads with an elastic thickness dependent on the new depth to the 450°C isotherm. In this section these conclusions are briefly examined in relation to the subsidence data along the seamount chain and to some results of flexure studies and gravity observations in the continents.

Deep drilling on atolls and volcanic islands in the Pacific indicate that there has been a significant subsidence of these features (for example, *Ladd and Schlanger* [1960], *Ladd et al.* [1967]) which cannot be explained by models in which they ride passively on the underlying lithosphere and subside as the lithosphere thickens and cools. Although the actual cause of this subsidence is unclear, three main hypotheses can be proposed: (1) viscous reaction of the lithosphere to the seamount loads, (2) subsidence following passage of the Pacific plate over a broad upwelling region in the underlying asthenosphere [*Menard*, 1973], and (3) subsidence due to lithospheric thinning following uplift of a broad shallow region associated with a hot spot [*Detrick and Crough*, 1978].

This study has shown that gravity and bathymetry data along the Hawaiian-Emperor seamount chain cannot be explained in terms of a simple viscoelastic model for the lithosphere. The problem then is how well the alternative hypotheses for the subsidence explain data along the chain. Although *Menard*'s [1973] is a plausible mechanism, it is difficult to test quantitatively. *Detrick and Crough* [1978], however, have shown that the mean depth of the sea floor adjacent to the seamount chain increases exponentially along the chain (from about 3800 m near Hawaii to about 5400 m near the Emperor Seamounts), suggesting a thermal origin for the subsidence.

The main difficulty with this hypothesis is the large amount of lithospheric thinning required to explain the observed subsidence. The elastic thickness estimates for the seamount chain can be explained by a simple thermal model for the cooling Pacific lithosphere (Figure 15) and do not require that the lithosphere was unusually thin at the time of loading. However, although the amount of the lithospheric thinning is presently unclear, this hypothesis could explain subsidence data along the seamount chain.

Owing to their geological complexity, it would not be expected that there would be any simple relationship between elastic thickness and age for the continents such as appears to exist for the oceans. However, surface loads in the continents have endured for the last 10^9 years, so the effect of viscous reaction of the continental lithosphere to these loads should be apparent in observed data.

Although there is a large scatter, there is some evidence that different age loads on Precambrian shield areas yield similar estimates of the elastic thickness of the continental lithosphere suggesting that there has been little or no viscous reaction of the continental lithosphere to long-term loads. *Walcott* [1970*b*] obtained a mean value for the flexural rigidity of the Precambrian basement at the Interior Plains and Caribou mountains loads of 4×10^{30} dyn cm, which corresponds to an elastic thickness of 40 km. The age of these loads is about 5×10^8 years [*Walcott*, 1970*b*]. Recently, *Haxby et al.* [1976] obtained a mean value for the flexural rigidity of the Precambrian basement underlying sediments in the Michigan basin of 4×10^{30} dyn cm. The age of this sediment load is approximately 3×10^8 years.

These conclusions are in general agreement with gravity observations in orogenic belts and over Precambrian granite plutons. First, there is a striking similarity in amplitude and wavelength of gravity anomalies over orogenic belts of widely different ages. For example, free air gravity anomaly profiles of the Appalachians [*Diment et al.*, 1972], where the main deformation is about 3×10^8 years, are strikingly similar to profiles of the Himalayas [*Gansser*, 1964], where the main deformation is about 2×10^7 years. The main features of these profiles are large-amplitude gravity highs (~120 mgal) over autochthonous regions of the central part of the orogenic belt and large-amplitude lows (~80 mgal) over the marginal thrusts and foreland regions. Second, large-amplitude gravity lows (~40 mgal) characterize high-level granite plutons in the Precambrian shield of North America (for example, *Garland* [1950]). If there was a significant viscous reaction to the stresses associated with orogeny and granite plutons, these gravity anomalies would be of small amplitude and show little or no correlation with surface geology.

Therefore, although there is still some uncertainty, there is evidence that a viscous reaction of the lithosphere to loads may not be occurring on a large scale in the continents, in agreement with the conclusions from the oceans. A viscous reaction to long-term loads may still occur in the continents, however, and further studies are required to examine this.

CONCLUSIONS

The analysis of gravity and bathymetry profiles of the Hawaiian-Emperor seamount chain allow the following conclusions to be made.

1. Cross-spectral techniques of analyzing gravity and bathymetry profiles over a single geological feature provide useful information on the state of isostasy at the feature.

2. Gravity and bathymetry profiles of the Hawaiian-Emperor seamount chain have been used to generate the transfer function or filter, which allows gravity to be predicted from bathymetry along the chain with a rms discrepancy of about ±15 mgal.

3. The resulting transfer function can be best explained by a simple model in which the Pacific oceanic lithosphere is treated as a thin elastic plate overlying a weak fluid. The best-fitting elastic thickness of the plate is in the range 20–30 km.

4. Analysis of individual gravity and bathymetry profiles show there are differences in the state of isostasy along the chain. Relatively high values for the elastic thickness were obtained for the Hawaiian Ridge and Emperor Seamounts south of 40°N, and relatively low values for the Emperor Seamounts north of 40°N.

5. The best explanation for these differences in the elastic thickness along the seamount chain is a simple model in which the elastic thickness depends on age and hence temperature gradient of the lithosphere at the time of loading. These differences along with estimates from other loads on young and old parts of the Pacific lithosphere suggest that the elastic thickness corresponds closely to the 450 ± 150°C oceanic isotherm.

6. The elastic thickness of the Pacific lithosphere does not appear to change appreciably through time. The large flexural stresses associated with the seamount loads therefore appear to be maintained for long periods of geological time, in qualitative agreement with subsidence data along the chain and with some gravity observations in the continents.

Acknowledgments. Steven Cande, Jim Cochran, John LaBrecque, Marc Langseth, Keith McCamy, and Dan McKenzie made a number of helpful suggestions and comments. This work was supported by National Science Foundation grant OCE 77-07941. The data used in this study were obtained mainly on cruises supported by the Office of Naval Research and National Science Foundation. Lamont-Doherty Geological Observatory Contribution No. 2744.

REFERENCES

Banks, R. J., R. L. Parker, and S. P. Huestis, Isostatic compensation on a continental scale: Local versus regional mechanisms, *Geophys. J. Roy. Astron. Soc., 51*, 431–452, 1977.

Barrell, J., The strength of the earth's crust, VIII, Physical conditions controlling the nature of lithosphere and asthenosphere, *J. Geol., 22*, 425–443, 1914.

Caldwell, J. G., W. F. Haxby, D. E. Karig, and D. L. Turcotte, On the applicability of a universal elastic trench profile, *Earth Planet. Sci. Lett., 31*, 239–246, 1976.

Chase, T. E., H. W. Menard, and J. Mammerickx, Bathymetry of the North Pacific, *Charts 1, 2, 3, 5, 6, 7*, Scripps Inst. of Oceanogr. and Inst. of Marine Resour., La Jolla, Calif., 1970.

Clague, D. A., and R. D. Jarrard, Tertiary Pacific plate motion deduced from the Hawaiian-Emperor chain, *Geol. Soc. Amer. Bull., 84*, 1135–1154, 1973.

Cochran, J. R., and A. B. Watts, An analysis of isostasy in the world's oceans, 2, Mid-ocean ridge crests, submitted to *J. Geophys. Res.*, 1978.

Dalrymple, G. B., M. A. Lanphere, and E. D. Jackson, Contributions to the petrology and geochronology of volcanic rocks from the Leeward Hawaiian Islands, *Geol. Soc. Amer. Bull., 85*, 727–738, 1974.

Den, N., W. J. Ludwig, S. Murauchi, J. I. Ewing, H. Hotta, N. T. Edgar, T. Yoshii, T. Asanuma, K. Hagiwara, T. Sato, and S. Ando, Seismic refraction measurements in the Northwest Pacific basin, *J. Geophys. Res., 74*, 1421–1434, 1969.

Detrick, R. S., and S. T. Crough, Island subsidence, hot spots, and lithospheric thinning, *J. Geophys. Res., 83*, 1236–1244, 1978.

Diment, W. H., T. C. Urban, and F. A. Revetta, Some geophysical anomalies in eastern North America, in *The Nature of the Solid Earth*, edited by E. C. Robertson et al., 544 pp., McGraw-Hill, New York, 1972.

Dorman, L. M., and B. T. R. Lewis, Experimental isostasy, 1, Theory of the determination of the earth's isostatic response to a concentrated load, *J. Geophys. Res., 75,* 3357–3365, 1970.

Dubois, J., J. Launay, and J. Recy, Some new evidence on lithospheric bulges close to island arcs, *Tectonophysics, 26,* 189–196, 1975.

Forsyth, D. W., The evolution of the upper mantle beneath mid-ocean ridges, *Tectonophysics, 38,* 89–118, 1977.

Furumoto, A. S., and G. P. Woollard, Seismic refraction studies of the crustal structure of the Hawaiian Archipelago, *Pacific Sc., 19,* 315–319, 1965.

Gansser, A., *Geology of the Himalayas,* 289 pp., John Wiley, New York, 1964.

Garland, G. D., Interpretations of gravimetric and magnetic anomalies on traverses in the canadian shield in northern Ontario, *Rep. XVI, No. 1,* 57 pp., Dep. of Mines and Tech. Surv., Dominion Observ., Canada, 1950.

Graf, A., and R. Schulze, Improvements on the sea gravimeter Gss 2, *J. Geophys. Res., 66,* 1813–1821, 1961.

Grow, J., and T. Atwater, Mid-tertiary tectonic transition in the Aleutian arc, *Geol. Soc. Amer. Bull., 81,* 3715–3722, 1970.

Gunn, R., A quantitative evaluation of the influence of the lithosphere on the anomalies of gravity, *J. Franklin Inst., 236,* 373–396, 1943.

Hanks, T. C., The Kuril trench–Hokkaido rise system: Large shallow earthquakes and simple models of deformation, *Geophys. J. Roy. Astron. Soc., 23,* 173–189, 1971.

Haxby, W. F., D. L. Turcotte, and J. M. Bird, Thermal and mechanical evolution of the Michigan Basin, *Tectonophysics, 36,* 57–75, 1976.

Hilde, T. W. C., Mesozoic sea-floor spreading in the North Pacific, Ph.D. thesis, Univ. of Tokyo, 84 pp., 1973.

Houtz, R. E., Seismic properties of layer 2A in the Pacific, *J. Geophys. Res., 81,* 6321–6331, 1976.

Jeffreys, H., *The Earth,* 438 pp. Cambridge University Press, New York, 1962.

Ladd, H. S., and S. O. Schlanger, Drilling operations on Eniwetok Atoll, *U.S. Geol. Surv. Prof. Pap., 260-Y,* 863–905, 1960.

Ladd, H. S., J. I. Tracey, and M. G. Gross, Drilling on Midway Atoll, Hawaii, *Science, 186,* 141–143, 1967.

Larson, R. L., and W. C. Pitman, World-wide correlation of Mesozoic magnetic anomalies and its implications, *Geol. Soc. Amer. Bull., 83,* 3645–3662, 1972.

Lewis, B. T. R., and L. M. Dorman, Experimental isostasy, 2, An isostatic model for the U.S.A. derived from gravity and topographic data, *J. Geophys. Res., 75,* 3367–3386, 1970.

McAdoo, D. C., J. G. Caldwell, and D. L. Turcotte, On the elastic perfectly plastic bending of the lithosphere under generalized loading with application to the Kuril trench, *Tectonophysics,* in press, 1978.

McKenzie, D. P., and C. Bowin, The relationship between bathymetry and gravity in the Atlantic Ocean, *J. Geophys. Res., 81,* 1903–1915, 1976.

Menard, H. W., Depth anomalies and the bobbing motion of drifting islands, *J. Geophys. Res., 78,* 5128–5137, 1973.

Munk, W. H., and D. E. Cartwright, Tidal spectroscopy and prediction, *Phil. Trans. Roy. Soc. Lond., Ser. A, 259,* 533, 1966.

Neidell, N. S., A statistical study of isostasy, *Geophys. Prospect., 11,* 164–175, 1963.

Parker, R. L., The rapid calculation of potential anomalies, *Geophys. J. Roy. Astron. Soc., 31,* 447–455, 1972.

Parsons, B., and P. Molnar, The origin of outer topographic rises associated with trenches, *Geophys. J. Roy. Astron. Soc., 45,* 707–712, 1976.

Parsons, B., and J. G. Sclater, An analysis of the variation of ocean floor bathymetry and heat flow with age, *J. Geophys. Res., 82,* 803–827, 1977.

Robertson, E. I., Gravity effects of volcanic islands, *New Zealand J. Geophys., 10,* 1466, 1967.

Robertson, E. I., Additional gravity surveys in the Cook Islands, *New Zealand J. Geophys., 13,* 184, 1970.

Shor, G. G., Crustal structure of the Hawaiian Ridge near Gardner Pinnacles, *Bull. Seismol. Soc. Amer., 50,* 563–573, 1960.

Tomoda, Y., and H. Kanamori, Tokyo surface-ship gravity meter α-1, in *Collected Reprints,* vol. 1, p. 116, Ocean Research Institute, University of Tokyo, 1962.

Vening, Meinesz, F.A., Gravity over the Hawaiian Archipelago and over the Madiera Area: Conclusions about the earth's crust, *Proc. Kon. Ned. Akad. Wetensch,* 44 pp., 1941.

Walcott, R. I., Flexure of the lithosphere at Hawaii, *Tectonophysics, 9,* 435–446, 1970*a*.

Walcott, R. I., Flexural rigidity, thickness, and viscosity of the lithosphere, *J. Geophys. Res., 75,* 3941–3954, 1970*b*.

Walcott, R. I., Lithospheric flexure, analysis of gravity anomalies, and the propagation of seamount chains, in *The Geophysics of the Pacific Ocean Basin and Its Margin, Geophys. Monogr. Ser.,* vol. 19, edited by G. H. Sutton, M. H. Manghnani, and R. Moberly, pp. 431–438, AGU, Washington, D. C., 1976.

Watts, A. B., Gravity and bathymetry in the Central Pacific Ocean, *J. Geophys. Res., 81,* 1533–1553, 1976.

Watts, A. B., and J. R. Cochran, Gravity anomalies and flexure of the lithosphere along the Hawaiian-Emperor Seamount Chain, *Geophys. J. Roy. Astron. Soc., 38,* 119–141, 1974.

Watts, A. B., and M. Talwani, Gravity anomalies seaward of deep-sea trenches and their tectonic implications, *Geophys. J. Roy Astron. Soc., 36,* 57–90, 1974.

Watts, A. B., J. R. Cochran, and G. Selzer, Gravity anomalies and flexure of the lithosphere: A three-dimensional study of the Great Meteor Seamount, northeast Atlantic, *J. Geophys. Res., 80,* 1391–1398, 1975.

Watts, A. B., M. Talwani, and J. R. Cochran, Gravity field of the northwest Pacific Ocean basin and its margin, in *Geophysics of the Pacific Ocean Basin and Its Margin, Geophys. Monogr. Ser.,* vol. 19, edited by G. H. Sutton, M. H. Manghnani, and R. Moberly, pp. 17–34, 1976.

Woollard, G. P., A gravity reconnaissance of the island of Oahu, *Eos Trans. AGU, 32,* 358, 1951.

Woollard, G. P., Crust and mantle relations in the Hawaiian area, in *Continental Margins and Island Arcs, Geol. Surv. Can. Pap., 66-15,* 294–310, 1966.

(Received February 24, 1978;
revised June 13, 1978;
accepted August 8, 1978.)